Full paper

A Complete System Modelling of Piezoelectric Energy Harvester (PEH) with Silicon Carbide (SiC) Used as Cantilever Base

Mohd Nor Fakhzan Mohd Kazim[a*], Selvanayakan Raman[a], Muhammad Hafiz Shafie[a], Nashrul Fazli Mohd Nasir[a], Asan Gani Abdul Muthalif[b]

[a]School of Mechatronic Engineering, Universiti Malaysia Perlis, Pauh Putra Campus, 02600 Arau, Perlis, Malaysia
[b]Department of Mechatronics, Kulliyah of Engineering, International Islamic University Malaysia (IIUM), 53100 Jalan Gombak. Kuala Lumpur, Malaysia

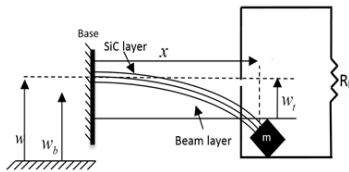*Corresponding author: fakhzan@unimap.edu.my

Graphical abstract

Abstract

Silicon carbide (SiC) is a material that possesses hardness and robustness to operate under high temperature condition. This work is a pilot in exploring the feasibility of cubic piezo element on the SiC wafer with integrated proof mass as horizontal cantilever with perpendicular displacement with respect to the normal plane. With the advance of electronic circuitry, the power consumption is reduced to nano-watts. Therefore, harvesting ambient energy and converting into electrical energy through piezoelectric material will be useful for powering low power devices. Resonance is a property which able to optimize the generated output power by tuning the proof masses. The damping ratio is a considerable parameter for optimization. From analytical study, small damping ratio will enhance the output power of the piezoelectric energy harvester (PEH). This paper will present mathematical modelling approach, simulation verification and the conditional circuit named versatile precision full wave rectifier.

Keywords: Silicon carbide; cantilever beam; piezoelectric; optimization, analytical modelling

∎1.0 INTRODUCTION

In recent years Micro Electro Mechanical Systems (MEMS) have been significantly impacted by the vibration energy harvester. This is in parallel with the development of low power wireless devices, which has prompted researchers to explore an alternative power supply which will enable the electronic devices to last longer. With such extensions, the applications of MEMS devices are toward wireless communication and sensors, where installation can be done at hard-to-reach locations [1]. To overcome location limitations, mechanical vibration from the surroundings is used for conversion into electrical energy.

Three different mechanisms, namely piezoelectric, electromagnetic and electrostatic, are used as converters. Of these three mechanisms, piezoelectric is the most reliable and is able to generate the maximum power for low power wireless electronic devices. Vibration is applicable either in the micro or macro size environmental area and it is essential for low or high temperatures. Robustness and working at high temperature are the main criteria in evaluating the harvester. Forty uniform energy harvesters have been tested at operating temperatures between 30°C and 100°C [2]. Further analysis has resulted in the fabrication of silicon carbide (3C-SiC) that can withstand temperatures of more than 500°C [3].

Various modelling methods have been presented in many research works to represent the estimated current, voltage and power output produced via the energy harvester. The beam thickness method is derived from the bending beam model [3]. Another modelling approach uses a rectangular plate based on Kirchhoff's assumption, where the equation of motion is referring to the flexural motion of the structure under the action of an applied electric field and external disturbance [4]. The simulation using the cantilever beam mode based on thin beam theory [5] was shown using different proof masses.

For practical implementation of piezoelectric energy harvesting (PEH), signal conditioning is used to define the overall efficiency of the power systems. In general, the piezo-element generates alternating current (AC) typically at a certain frequency and the load requires a direct current (DC) supply. The purpose of obtaining DC voltages is to ensure that the energy from the piezo-element will able to power up the low power devices. Four diodes are used as a Wheatstone bridge which converts the AC to DC. However, the rectification process for the main technique is performed by an operational amplifier and not by diodes [7].

A precise rectification function is an important requirement in many applications such as instrumentation and measurement. The precision of the rectification circuit is obtained by using certain components such as a high performance amplifier. Due to the need for precise rectification, a precise rectifying circuit is

proposed, consisting of an all-pass filter that acts as a 90° phase shifter, two squaring circuits, one summer, and one square rooter. The sinusoidal signal is shifted by adjusting the resistance and capacitance. This paper investigates the performance of power conditioning strategies and the design of a power conditioning circuit that produces stable DC output.

For a high-precision rectifying circuit using an all-pass filter that acts as a 90° phase shifter, it is reported by the previous researchers that an operational amplifier with a specific current conveyor is used due to the high output impedance of the current conveyor to overcome the turn-on resistance of the diode, permitting the rectification of low-level signals and also responding to frequencies over 100 kHz [8].

The vibration suppression techniques use a piezoceramic actuator coupled to a switching circuit where a synchronized switch controls the energy flow through the switching shunt network between the low short circuit and high open circuit stiffness. As a result, the targeted structure motion is attenuated because the shunt circuit absorbs the converted electrical energy obtained by transduction of mechanical energy [9].

This article will discuss the analytical modelling of an SiC cantilever beam using the thin beam approach to estimate the frequency response function (FRF) of the output voltage. Secondly, the beam with different proof masses will be discussed. Then, we will look at the conditional circuit which is designed in order to boost the generated output voltage. And finally, this paper will conclude based on the performance of the SiC cantilever piezoelectric with the best output produced under extreme environment conditions.

■2.0 MATHEMATICAL MODELLING

2.1 Thin Beam-Theory

A 2D model of a unimorph piezoelectric cantilever beam (Figure 1) is made of a piezoelectric layer sandwiched between substrate layers as the top and bottom electrodes. This fix-free beam is defined fixed and free end. The beam variables are defined as:

L = length of the beam
w = width of the beam
h = beam thickness
h_p = piezoelectric thickness.
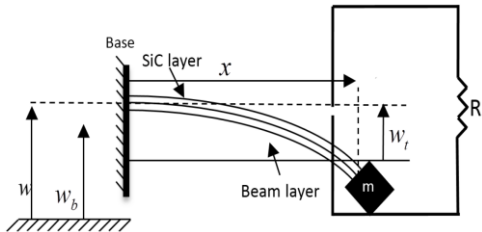
Figure 1 SiC energy harvester with tip mass under transverse base motions

The beam equation of motion is derived according to the thin beam theory as

$$\frac{\partial^2 M}{\partial x^2}(x,t) + \rho A(x)\frac{\partial^2 w}{\partial t^2}(x,t) = f_0(x,t) \tag{1}$$

where:
r = mass density

A = cross-sectional area
M (x,t) = moment;

$$w(x,t) = w_b(t) + w_t(x,t) \tag{2}$$

where:
w(x,t) = total displacement of the beam
$w_b(t)$ = base displacement
w_t (x,t) = beam transverse displacement with response to the base;

the external force due to the surrounding vibration to the beam is expressed as

$$f(t) = -\rho A(x)\frac{\partial^2 w_b(t)}{\partial t^2} \tag{3}$$

Hence, by inserting Equation (2) and (3) into Equation (1), it becomes

$$\frac{\partial^2 M(x,t)}{\partial x^2} + \rho A(x)\frac{\partial^2 \left(w_t(x,t)\right)}{\partial t^2} = -\rho A(x)\frac{\partial^2 \left(w_b(t)\right)}{\partial t^2} \tag{4}$$

In Equation (1), M(x,t) is the moment at the beam which is defined from the general beam equation. If a piezoelectric patch is attached to the beam, the moment will change due to the additional piezoelectric effect. When external load is applied to the beam, it deflects downward and the piezoelectric patch placed above the neutral axis experiences tension.

The relation between mechanical stress and piezoelectric strain is expressed by using the piezoelectric constitutive equation:

$$D_3 = d_{31}\sigma + \varepsilon_{33}^T E_3 \tag{5}$$

where:
D_3 = electrical displacement
d_{31} = piezoelectric strain constant
σ = stress
ε_{33}^T = permittivity at constant stress
E_3 = applied electric.

The value of ε_{ij}^S is obtained accurately by using the equation below:

$$\varepsilon_{33}^T - \varepsilon_{33}^S = d_{31}E_P \tag{6}$$

In the piezoelectric element, electric charges $\bar{Q}(t)$ develop; this is obtained by integrating the electric displacement over the beam area:

$$\bar{Q}(t) = \int_A D.ndA$$
$$= -\int_{x=0}^{L} d_{31}E_P\left(\frac{h}{2}+h_p\right)B\frac{\partial^2 w_t(x,t)}{\partial x^2}dx + \varepsilon_{33}^T BL\frac{v(t)}{h_p} \tag{7}$$

The current is calculated by differentiating the charge with respect to time.

$$i(t) = \frac{d\bar{Q}(t)}{dt}$$
$$= -\int_{x=0}^{L} d_{31}E_P\left(\frac{h}{2}+h_p\right)B\frac{\partial^2 w_t(x,t)}{\partial x^2}dx - \frac{\varepsilon_{33}^T}{h_p}BL\frac{dv(t)}{dt} \tag{8}$$

Therefore, the voltage output is measured as follows:

$$\frac{\varepsilon_{33}^T}{h_p}BL\frac{dv(t)}{dt} + \frac{v(t)}{R_l} = -\int_{x=0}^{L} d_{31}E_P\left(\frac{h}{2}+h_p\right)B\frac{\partial^2 w_t(x,t)}{\partial x^2}dx \tag{9}$$

where R_l is the resistive load.

The shape of the beam is defined by W_{tn} and $q_{tn}(t)$ defines the vibration of the beam. $W_{tn}(x)$ is the Eigen function representing the nth mode shape corresponding to the undamped free vibration problem:

$$W_{tn}(x) = C_{1n}\left[\left(\sin\beta_i x - \sinh\beta_i x\right) - \alpha\left(\cos\beta_i x - \cosh\beta_i x\right)\right] \quad (10)$$

where

$$\alpha = \frac{\sin\beta_i l + \sinh\beta_i l}{\cos\beta_i l + \cosh\beta_i l} \quad (11)$$

where β_i's are the dimensionless frequency number obtained from the frequency equation given by

$$1 + \frac{1}{\cos\beta l \cosh\beta l} - R\beta l\left(\tan\beta l - \tanh\beta l\right) = 0 \quad (12)$$

where R is expressed as

$$R = \frac{M}{\rho Al} \quad (13)$$

The amplitude of the output voltage is represented by

$$|V_0| = \frac{\tau_c \omega^3 \varphi_{tn}(t) \int_0^l W_t(x)\,dx}{\sqrt{\left[\omega_{ni}^2 - \omega^2\left(1 + 2\zeta_{nk}\tau_c\omega_{ni}\right)\right]^2 + \left[2\zeta_{nk}\omega_{ni}\omega + \tau_c\omega\left(\varphi_{tn}\dfrac{\vartheta}{\rho A} + \omega_{ni}^2 - \omega^2\right)\right]^2}} w_l$$

$$(14)$$

$$\varphi_{tn} = -\frac{d_{31}E_p h_p\left(\dfrac{h}{2} + h_p\right)}{\varepsilon_{33}^T L}\int_{x=0}^{L}\frac{\partial^2 W_{tn}(x)}{\partial x^2}\,dx \quad (15)$$

$$\tau_c = \frac{R_l\varepsilon_{33}^T BL}{h_p} \quad (16)$$

The damping ratio value used for the simulation is measured from the experiment [1] in order to obtain reasonable results. Equations (14) to (16) state that the output voltage produced depends on the beam dimension, smart material properties and proof mass applied.

2.2 Cantilever Properties

The beam is modelled as a fix-free beam with a piezoelectric layer and non-piece layer. The length and width of the cantilever are 400 mm and 30 mm respectively, the thickness of each layer is 1 mm and it is pulled along the z-axis.

An analysis is done to estimate the output in terms of the voltage frequency response function (FRF). Different proof masses and modes of the beam are analysed and discussed.

Table 1 Parameters of SiC PEH beam

Parameter	SiC	Unit
Length	400	μm
Width	30	μm
Thickness (green, violet red, red, Si substrate)	173	μm
Type	n	-
Density	3.21	g/m³
Young's modulus	748	GPa
Poisson's ratio	0.14	-
Fracture toughness	4.6	Mpa.m^{1/2}
Hardness	2800	GPa
Flexural strength	550	Mpa
Energy band gap	236	eV
Maximum use temperature (no load)	1650	°C

2.3 Analysis of Voltage Produced by the PEH

The voltage generated by the PEH is calculated from the voltage Equation (14). The analytical results were plotted with w_{b0} assumed to be 2.3 x 103. The $\beta_i l$ is taken from the first mode of the beam shape which 1.8752, the first natural frequency of the beam is 1202.96 Hz, and the integral value of w_t is equal to 0.0038. The f value is equal to -4944 x 10⁻⁸. The time constant value is calculated to be 138. Analysis was performed with damping values of 0.05x10⁻⁶. The voltage given by Equation (14) is plotted in Figure 2, where the amplitude of the voltage decreases with increasing natural frequency. The maximum voltage obtained for the first mode excitation is 6.175μV and the second mode excitation is 0.06075μV.
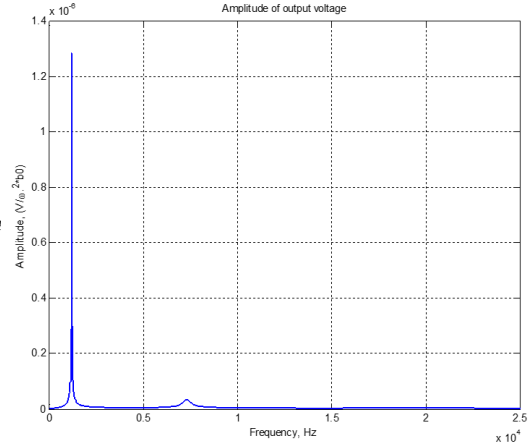
Figure 2 Simulated output voltage for first three resonances for SiC cantilever beam

2.4 Analysis of PEH with Variable Proof Masses

The PEH was also tested with variable tip masses to enhance the generated output voltage. The simulation results for the output voltage tested with variable proof mass are also presented in Figure 3. From the analytical results, increase of the proof mass will contribute higher output voltage and decrease the beam's natural frequency. As seen from Figure 3, the simulated output voltage is increased from 1.282 mV to 2.945 mV with mass added. The voltage produced is gradually increased to 4.655 mV with two masses added, and 6.175 mV with three masses.

Instead of an increase of output voltage, the 1st natural frequency of the beam with no mass is 1202.96 Hz. The value decreases to 790.91 Hz when one proof mass is added. The beam was tuned to be 630.43 Hz with two proof masses added and finally the resonance frequency decreased to 539.76 Hz when three proof masses were added to the beam. In the simulation the PEH works with a frequency range from 0 to 10 kHz. The additional proof masses in the developed PEH decrease its natural frequency. This condition holds true if the beam is working under the elastic region and the proof mass does not exceed its fracture point. However, if the proof mass is loaded exceeding its limit, the beam will fall into the plastic region.

The second analysis is done to observe the trend of the proof mass with the generated output voltage. Table 2 shows the proof masses with output voltage at the 1st and 2nd natural frequencies. From the simulation results, the increment of proof masses affects the output voltage generated in the 2nd mode.
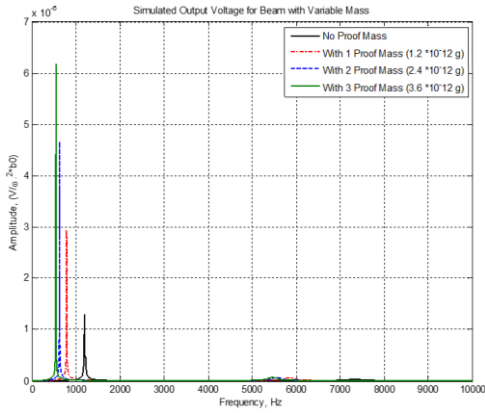
Figure 3 Simulated output voltage with variable masses

Table 2 Simulated output voltage for variable proof masses

Number of masses	Simulated output voltage	
	1st mode	2nd mode
No mass	1.282 µV	0.05339 µV
1 mass - 1.2 x 10^{-12}g	2.945 µV	0.05278 µV
2 masses - 2.4 x 10^{-12}g	4.655 µV	0.05822 µV
3 masses – 3.6 x 10^{-12}g	6.175 µV	0.06075 µV

The operating frequency is between 5 kHz and 6 kHz for 1, 2 and 3 masses. However, for the no mass beam, the 2nd mode is around 7.2 kHz.
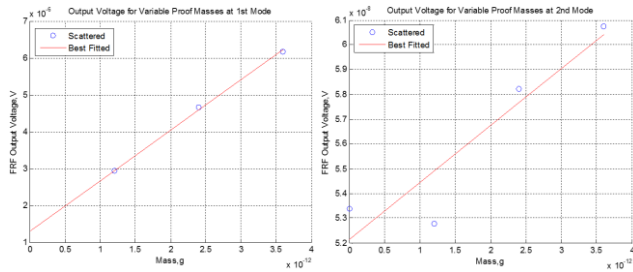

Figure 4 Simulated output voltage versus variable proof masses for SiC cantilever beam

The graph in Figure 4 shows a linear relation between the output voltages. The result is obtained with three different proof masses. The FRF of the output voltage is measured at the resonance at the first mode for all three proof masses. At the beginning of Figure 4, no mass is added and the output voltage produced is 1.282 mV, and with three masses the output voltage produced is 6.175 mV. The FRF voltage produced at the 2nd mode shows a scattered plot against the masses. From Figure 4, the output voltage, 0.05278 mV, with 2 proof masses is the only point which is below the red line, while the others are above the red line. From the simulation, it is found that adding mass increases the generated output voltage up to a certain limit.

■**3.0 ELECTRONIC SIMULATION**

The efficiency of the energy harvester is analysed with the conditioner circuit where the amount of energy extracted and stored is measured. The software Multisim 10.0 by National

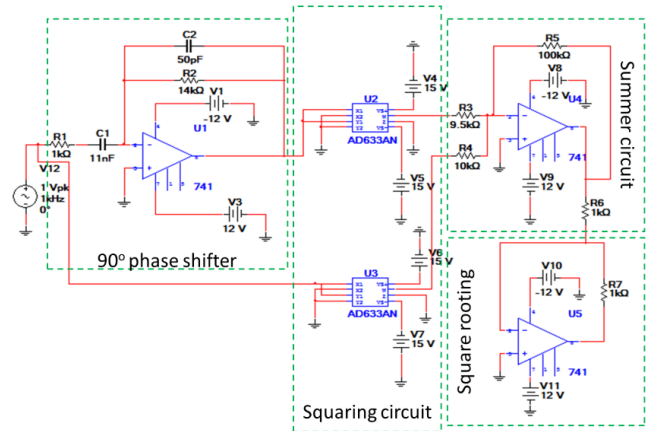Instrument is used to simulate the energy extraction and storing from the PEH.

Figure 5 A versatile full wave rectifier circuit

Figure 5 shows a rectification circuit of versatile precision which produces full wave rectified output. The circuit consists of four main parts:
 a) all-pass filter that acts as a 90° phase shifter
 b) two squaring circuits
 c) one summer
 d) one square rooter.

The phase of the input sinusoidal signal is given by $V_{in} = A \sin (2\pi ft)$ where amplitude, A and frequency, f are shifted by 90° by using the all-pass filter and adjusting the resistance, R and capacitance, C of the RC network. The combination of the RC network and all-pass filter keeps the 90° phase shifted amplitude equal to the amplitude of the input signal.
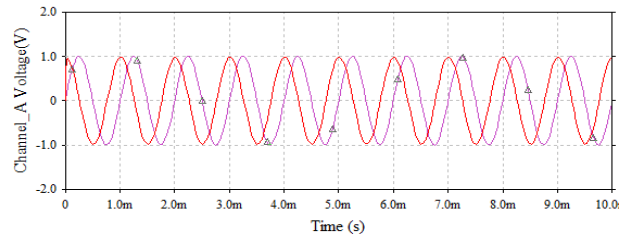

Figure 6 90° phase shifted waveform

To maintain the phase shift of 90° as in Figure 6 for different frequencies, R and C are adjusted accordingly. The output signal of the phase shifter circuit can be written as $V_p = A \sin (2\pi ft)$. The squaring of V_{in} and V_p is done by using analog multiplier AD 633, as shown in Figure 7. After the squaring process, these squared signals are summed by using the op-amp UA741 that connects in series with the square rooting circuit which consists of another UA741 op-amp. After the square rooting process, the signal produces a rectified output of $V_{out} = A$.
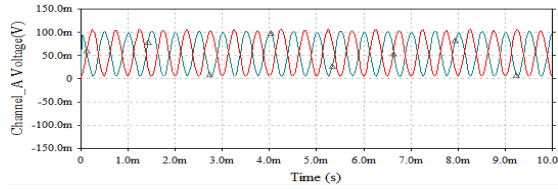
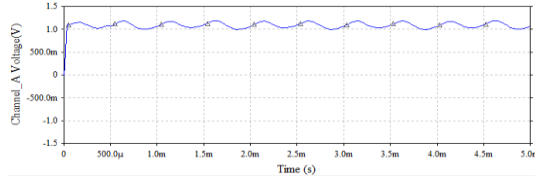**Figure 7** Squaring waveform of both input signal and phase shifted signal

Figure 8 Rectified output waveform of the main circuit

Table 3 Output power of versatile precision full wave rectifier circuit

R_L (Ω)	V_{DC} (V)	I_{DC}(A)	P_{DC} (W)
100	0.11	0.0011	0.00012
200	0.219	0.001095	0.00024
300	0.327	0.00109	0.00036
400	0.436	0.00109	0.00048
500	0.545	0.00109	0.00059
600	0.653	0.001088	0.00071
700	0.762	0.001089	0.00083
800	0.871	0.001089	0.00095
900	0.98	0.001089	0.00107
1000	1.09	0.00109	0.00119

3.1 Waveform Analysis

Two waveforms are provided as a result of the combination of specific circuits of a versatile precision full wave rectifier. Figure 6 shows the 90° phase-shifted waveform that is the same as the peak input signal. The waveform in Figure 7 is produced from the squaring of the input signal and the output of the phase shifter circuit. It is seen that the waveform is squeezed with respect to the time-based scale because the frequency is doubled. Finally, the waveform in Figure 8 is the rectified output of the main circuit which produces less rippled voltage. Based on the graph produced, it can be concluded that the DC voltage depends on the supply input and the resistive load value itself. The circuit will generate high DC voltage as the circuit is supplied by high input AC voltage. Moreover, from the formula of $V=IR$, it indicates that the circuit will produce high DC voltage as the value of resistor, R of the resistive load (resistor at probing part) is high.

3.2 Transfer Function

The transfer function characteristic of the proposed circuit is studied for a lower frequency of 50 Hz and higher frequency of 1 kHz. We have used a 280 kΩ resistor and 50 pF capacitor at 50 Hz frequency, and a 14 kΩ resistor and 50 pF capacitor at 1 kHz frequency. These specific values of frequencies and components are able to maintain a 90° phase shift off the all-pass filter. At frequencies of 50 Hz and 1 kHz, the value of the rectified output voltage obtained is almost the same as the peak input voltage. The amplitude of the sinusoidal signal and 90° phase-shift into the cosine signal is kept the same by the AD741 all-pass filter. Thus, it is confirmed from the transfer characteristics that the circuit performs well at both lower and higher frequencies.

3.3 Power harvested

The harvested power is calculated by measuring the rectified voltage on a variable resistive load from 100 Ω to 1 kΩ. Then the measured voltage, V_{DC} is inserted into:

$$I_{dc} = \frac{V_{dc}}{R} \tag{17}$$

The harvested power can be obtained from the power formula of:

$$P = I_{dc}^2 \times R \tag{18}$$

The table above shows the data of the main circuit that is obtained by measurement and calculation. Table 2 shows that all the parameters are proportional to the resistive load value, R_L. This means that the main circuit can harvest much energy from the high voltage system.

■4.0 RESULTS AND DISCUSSION

The harvested power traces of the main technique increase linearly, while other techniques showed decreases of their harvested power. Figure 9 shows that with the standard technique with transformer and without capacitor, the harvested power increases until a certain resistive load value before it decreases for higher resistive loads. However, low rectified voltage values also cause the efficiency of the converter to decrease due to high current values through the inductor and capacitor respectively, thus increasing resistive losses.
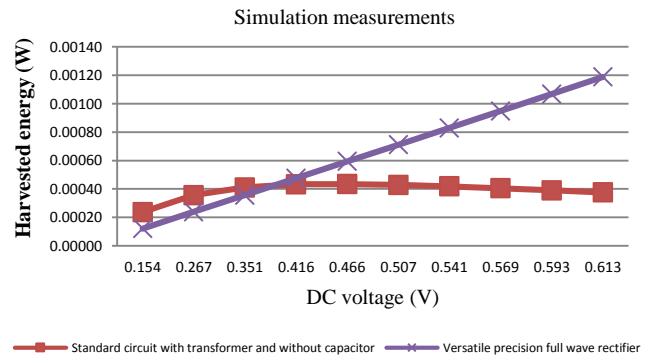

Figure 9 The simulated measurement of harvested power with respect to DC voltage

■5.0 FUTURE RECOMMENDATIONS AND CONCLUSIONS

Piezoelectric is a promising energy harvester which can devour the energy needed for use by small electrical appliances. This paper performs mathematical modelling analysis of a cantilever structure on SiC with proof mass added to the end of the beam. The generated FRF output voltage depends on the beam parameter and also the force applied to the beam. Our simulation shows that

the generated output voltage at 1KW will increase with increased proof mass.

To optimize the output of the energy harvester it is recommended to vary the beam shape to increase the stress and strain area of the deflected beam. Next is to validate the output voltage with experimentation, where the setup will involve a dynamic checker and an accelerometer, and it is recommended to use laser Doppler as the SiC beam is of a micro size. It is recommended that the size of the SiC should be reduced since thicker sizes will affect the beam's natural frequencies.

As a conclusion for the conditional parts, a basic circuit and a precision full-wave rectification technique using an all-pass filter as a 90° phase shifter are presented. The basic circuit gives stable DC output voltage because of its smoothing capacitor. The output voltage amplitude is higher than the input voltage at 200 Hz.

The rectified output of the circuit with transformer depends on the coil inductance of the primary and secondary coil. Furthermore, the precision full wave circuit also provides stable DC output voltage, which seems to have less ripple voltage at a low frequency of 50 Hz and greater ripple voltage at the higher frequency of 1 kHz. However, this maintains the phase shift whenever frequency is supplied into the circuit as the circuit uses an operational amplifier. Based on the graph, the harvested power of the main technique is proportional to the DC voltage.

References

[1] J. M. Gilbert and F. Balouchi. 2008. Comparison of Energy Harvesting Systems for Wireless Sensor Networks. *International Journal of Automation and Computing*. 5(4): 334–347.

[2] R. Xu, L. M. Borregaard, A. Lei, M. Guizzetti, E. Ringgaard, T. Zawada, O. Hansen, and E. V. Thomsen. 2012. Preliminary Performance Evaluation of MEMS-based Piezoelectric Energy Harvesters in Extended Temperature Range. *Procedia Engineering*. 47: 1434–1437.

[3] J. M. R. Kudimi, F. Mohd-Yasin, and S. Dimitrijev. 2012. SiC-based Piezoelectric Energy Harvester for Extreme Environment. *Procedia Engineering*. 47: 1165–1172.

[4] Y. Li, L. Cheng, and P. Li. 2003. Modeling and Vibration Control of a Plate Coupled with Piezoelectric Material. *Composite Structures*. 62(2): 155–162.

[5] M. N. Fakhzan and A. G. A. Muthalif. 2011. Vibration based Energy Harvesting Using Piezoelectric Material. In Mechatronics (ICOM), 2011 4th International Conference On. 1–7.

[6] M. N. Fakhzan and A. G. A. Muthalif. 2013. Harvesting Vibration Energy Using Piezoelectric Material: Modeling, Simulation and Experimental Verifications. *Mechatronics*. 23(1): 6–66.

[7] S. J. G. Gift and B. Maundy. 2007. Versatile Precision Full-Wave Rectifiers for Instrumentation and Measurement. *IEEE Trans. Instrum. Meas.* 56(5): 1703–1710.

[8] Clark, W. W. 1999. Semi-active Vibration Control with Piezoelectric Materials as Variable Stiffness Actuators. Proceedings of SPIE-The International Society for Optical Engineering. 3672: 123–130.

[9] L. R. Clare, S. G. Burrow. 2008. Power Conditioning For Energy Harvesting. *Active and Passive Smart Structures and Integrated Systems*. 6928.

[10] Henry A. Sodano, Daniel J. Inman and Gyuhae Park. 2004. A Review of Power Harvesting from Vibration Using Piezoelectric Materials. *Center For Intelligent Material Systems and Structures*. 36(3): 197–205.

[11] Lallart. M., Garbuio. L., Richard. C, Guyomar. D. 2008. Double Synchronized Switch Harvesting (DSSH). A New Energy Harvesting Scheme For Efficient Energy Extraction. *IEEE Trans Ultrasonic Ferroelectric Frequency Control*. 55(10).

[12] Geffrey K. Ottman, Heath F. Hofmann and George A. Lesieutre. 2003. Optimized Piezoelectric Energy Harvesting Circuit Using Step-down Converter in Discontinuous Conduction Mode. *IEEE Trans. Power Electron.* 18: 696–703.

[13] Mahmoud, K. M. Younis, Mohd Zulfadhli Ahmad Marzuki. 2010. Cantilever Beam Vibrations into Useful Energy. Final Year Project Report: UIAM.

[14] A. K. A. Mohd Ihsan, H. A. Lim, and M. J. Mohd Nor. 2012. Analysis, Design and Simulation of Piezoelectric Acoustic Microsensor. *J. Teknol.* 44(1): 13–26.

[15] N. M. Nor Ayob, M. J. Pusppanathan, R. Abdul Rahim, M. H. F. Rahiman, F. R. Mohd Yunu, S. Buyamin, I. M. Abd Rahim, and Y. Md Yunos. 2013. Design Consideration for Front-End System in Ultrasonic Tomography. *J. Teknol.* 64(5).